















Effects of material properties of band-gap-graded Cu(In,Ga)Se₂ thin films on the onset of the quantum efficiency spectra of corresponding solar cells

Sinju Thomas¹ | Tobias Bertram²  | Christian Kaufmann²  | Tim Kodalle²  | José A. Márquez Prieto¹  | Hannes Hempel¹  | Leo Choubrac¹  | Wolfram Witte³  | Dimitrios Hariskos³  | Roland Mainz¹  | Romain Carron⁴  | Jan Keller⁵  | Pablo Reyes-Figueroa²  | Reiner Klenk²  | Daniel Abou-Ras¹ 

¹Helmholtz-Zentrum Berlin für Materialien und Energie GmbH, Berlin, Germany

²Helmholtz Zentrum Berlin für Materialien und Energie GmbH, Competence Centre Photovoltaics Berlin (PVcomB), Berlin, Germany

³Zentrum für Sonnenenergie- und Wasserstoff-Forschung Baden-Württemberg (ZSW), Stuttgart, Germany

⁴Empa - Swiss Federal Laboratories for Materials Science and Technology, Dübendorf, Switzerland

⁵The Angström Laboratory Solar Cell Technology, University of Uppsala, Uppsala, Sweden

Correspondence

Sinju Thomas, Helmholtz-Zentrum Berlin für Materialien und Energie GmbH, Hahn-Meitner-Platz 1, 14109 Berlin, Germany.
Email: sinju.thomas@helmholtz-berlin.de

Funding information

Bundesministerium für Wirtschaft und Klimaschutz (BMWK), Grant/Award Numbers: 03EE1059A(ZSW), 03EE1059B(HZB)

Abstract

Polycrystalline Cu(In,Ga)Se₂ (CIGSe) thin-film solar cells exhibit gradual onset in their external quantum efficiency (EQE) spectra whose shape can be affected by various CIGSe material properties. Apart from influences on the charge-carrier collection, a broadening of the EQE onset leads to enhanced radiative losses in open-circuit voltage (V_{oc}). In the present work, Gaussian broadening of parameters describing the EQE onset of thin-film solar cells, represented by the standard deviation, σ_{total} , was evaluated to study the impacts of the effective band-gap energy, the electron diffusion length, and the Ga/In gradient in the CIGSe absorber. It is shown that σ_{total} can be disentangled into contributions of these material properties, in addition to a residual component $\sigma_{residual}$. Effectively, σ_{total} depends only on a contribution related to the Ga/In gradient as well as on $\sigma_{residual}$. The present work highlights the connection of this compositional gradient, the microstructure in the polycrystalline CIGSe absorber, and the luminescence emission with the residual component $\sigma_{residual}$. It is demonstrated that a flat band-gap with no compositional gradient in the bulk of the CIGSe absorber is essential to obtain the lowest σ_{total} values and thus result in lower recombination losses and gains in V_{oc} .

KEYWORDS

band-gap fluctuations, Cu(In, Ga)(Se,S)₂, external quantum efficiency, gradient

1 | INTRODUCTION

Cu(In,Ga)Se₂ (CIGSe) thin-film solar cells (front contact/CIGSe/Mo/glass stacks) with record conversion efficiencies of more than 23%¹ exhibit Ga/In gradients with higher [Ga] towards the back and higher [In] towards the front contact. Since the band-gap energy (E_g) of

CuInSe₂ (1.04 eV)² is smaller than that of CuGaSe₂ (1.68 eV), the varying $[Ga]/([Ga] + [In])$ (GGI) ratio perpendicular to the substrate leads to a variation of the local E_g in the solid solution CIGSe.² The GGI gradients in CIGSe layers for high-efficiency devices (>20%) exhibit V-shapes with a local minimum of [Ga] and thus of E_g at a position between front and back contact. This position (on an axis

This is an open access article under the terms of the [Creative Commons Attribution](https://creativecommons.org/licenses/by/4.0/) License, which permits use, distribution and reproduction in any medium, provided the original work is properly cited.

© 2022 The Authors. Progress in Photovoltaics: Research and Applications published by John Wiley & Sons Ltd.

perpendicular to the substrate) is what determines the onset of the light absorption as a function of the photon energy, and the minimum or effective E_g of a graded CIGSe thin film can be obtained from the onsets in absorption or in external quantum efficiency (EQE) spectra.

While the evaluation of absorption spectra offers the advantage of the absence of any transport-related effects (which need to be taken into account in EQE spectra), such measurements cannot be performed easily on completed solar cells owing to the opaque Mo back contact. Since CIGSe layers on transparent substrates need not to exhibit the identical materials properties as those in completed solar cells with Mo/glass substrates, it is not possible to correlate directly the absorption behavior of a CIGSe layer on a transparent substrate with the device performance of the front contact/CIGSe/Mo/glass solar cell. Therefore, the absorption behaviors of CIGSe layers were investigated by the evaluation of EQE spectra of the corresponding solar cells with Mo back contacts in the present work.

Onsets of the EQE spectra are not only affected by charge-carrier transport.³ Other contributing factors are the CIGSe film thickness, as well as E_g fluctuations in the CIGSe alloy.⁴ The shape of the EQE onset has an impact on the V_{oc} via radiative losses and on the collection.⁵ However, it is unclear whether E_g fluctuations can be determined easily by evaluation of the onset in EQE spectra for solar cells with various CIGSe layer thicknesses (in case transport effects can be neglected). We note that in the following, the CIGSe compound with $x = \text{GGI}$ exhibits a band-gap energy $E_g(x) = (1-x) E_g(\text{CuInSe}_2) + x E_g(\text{CuGaSe}_2) - bx(1-x)$, where $b = 0.2$ is the bowing parameter.⁶

In the present work, the onset of the EQE spectra of CIGSe solar cells with varying effective E_g and Ga gradients was evaluated by fitting Gaussians to the first derivatives of the EQE spectra, which provides the effective E_g values from the mean and σ_{total} from the standard deviations of the Gaussians.^{7,8} We will show that the influence of the CIGSe layer thickness, low diffusion length and Ga gradient on the shape of the EQE onset is substantial. In order to facilitate optimal carrier collection and reduced radiative V_{oc} losses, compositional gradients in CIGSe layers should be restricted to the regions close to the interfaces to the front and back contacts.

2 | EVALUATION OF THE ONSET IN EQE SPECTRA

The onset of an EQE spectrum can be evaluated in various ways. One possible and established approach is to extract the Urbach energy (E_u) from the subgap region of the internal QE (IQE) spectrum, which needs the input of the EQE and reflectance R spectra, since $\text{IQE}(E) = \text{EQE}(E) / (1-R(E))$ (E is the photon energy).⁹ The E_u is then given as the inverse of the slope of the subgap region in the IQE spectra (i.e., $\ln(\text{IQE}(E)) = c + E/E_u$, where c is a constant).⁹

Yet another way is to evaluate not $\text{EQE}(E)$ but its first derivative $d\text{EQE}/dE$ to obtain a E_g distribution as proposed by Rau et al.⁷ followed by a Gaussian fitting of the E_g distribution.^{8,10} A Gaussian (Figure 1, green curve) is fitted to the function $d\text{EQE}/dE$ (Figure 1, red curve) around its local maximum. According to Rau et al., the mean of

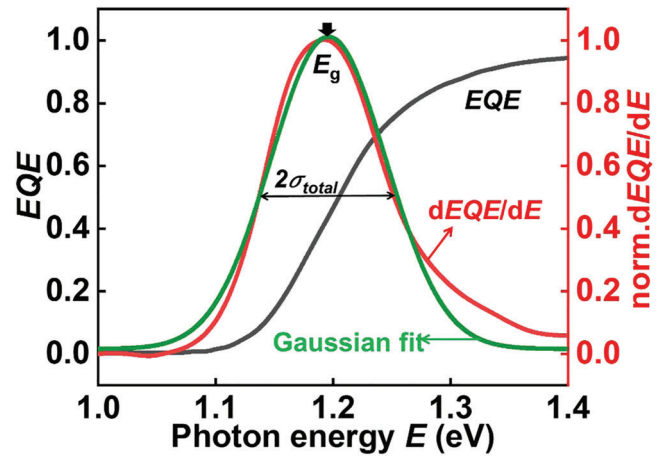


FIGURE 1 Experimental external quantum efficiency (EQE) spectrum (black) for one of the solar cells studied in the present work. Gaussian fitting (green) of the first derivative of EQE (red) (normalized to 1) gives an effective band-gap energy $E_g = 1.19$ eV as mean and σ_{total} of 49 meV as standard deviation

the Gaussian gives the effective band-gap energy E_g of the solar absorber, and the standard deviation the amplitude of band-gap fluctuations (σ_g), when electrostatic potential fluctuations can be neglected.^{4,8,11} It is visible in Figure 1 that the Gaussian fit deviates substantially from the experimental $d\text{EQE}/dE < 0.3$ (normalized). Nevertheless, the fit agrees well with the experimental data for $d\text{EQE}/dE > 0.3$ (normalized), at the center of the peak and FWHM which is where the effective (E_g) and the standard deviation (σ_{total}) are extracted.

Unfortunately, this scenario is too simple, since EQE onset is known to be affected considerably by the electron diffusion length in the absorber and by the absorber thickness.^{3, 12-15} It will be an essential part of the present work to disentangle the standard deviation σ_{total} (determined by the Gaussian fit) to obtain its contributions by the diffusion length (σ_{diff}), the (effective) absorber thickness (σ_{thick}), the E_g gradient (σ_{grad}), and a residual component (σ_{residual}).

A straightforward approach would be to consider these individual quantities as independent contributions to σ_{total} : $\sigma_{\text{total}}^2 = \sigma_{\text{diff}}^2 + \sigma_{\text{thick}}^2 + \sigma_{\text{grad}}^2 + \sigma_{\text{residual}}^2$. However, in a real CIGSe solar cell, these contributions are not independent from one another. Indeed, the Ga/In gradient affects considerably the effectively light-absorbing thickness of the CIGSe layer. Also, the Ga/In gradient may influence the diffusion length of the charge carriers, for example, in case it exhibits a decreasing GGI from the Mo/CIGSe interface towards the CIGSe/buffer interface (since then, electrons are repelled from the back contact). At any rate, when regarding CIGSe solar cells with absorbers free of any band-gap gradient, it becomes clear that the impact of σ_{diff} and σ_{thick} on σ_{total} can be neglected (see supporting information S1 and S2). Since the present work deals only with graded CIGSe absorbers, σ_{grad} contains contributions also of σ_{diff} and σ_{thick} , and σ_{total} can be expressed via:

$$\sigma_{\text{total}}^2 = \sigma_{\text{grad}}^2 + \sigma_{\text{residual}}^2 \quad (1)$$

It is important to note that an experimental EQE spectra exhibit influences of the subgap absorption, the diffusion length, and the effective thickness of the absorber, leading to a Gaussian-type $dEQE/dE$ curve with standard deviation σ_{total} . In contrast, when simulating the effects of only the E_g gradient on the EQE onset, no Gaussian-type distribution $dEQE/dE$ is obtained. A corresponding Gaussian fit for the determination of the standard deviation seems to be inappropriate at first glance. However, in the present work, we will simply use the Gaussian fit as a tool to quantify the broadening of the $dEQE/dE$ curve and to be able to determine eventually the residual broadening σ_{residual} in Equation (1).

This residual broadening will be related (mainly) to local strain and/or compositional variations in the polycrystalline CIGSe layer. These variations are present at various length scales (0.1 nm to 1 μm^4) and can, unfortunately, not always be assessed easily via microscopic analyses; however, they were detected and quantified at grain boundaries and dislocations in polycrystalline CIGSe.^{5,16} What we assume is that the local strain and/or compositional variations induce corresponding changes in the electronic structure, that is, in the conduction-band and valence-band edges, and thus lead to local variations of E_g , that is, to E_g fluctuations.¹⁷

For all the solar cells studied in the present work, the EQE spectra feature subgap absorption visible as band tails (at $E < E_g$) at the EQE onset. The Urbach energies (E_u) were determined from all experimental EQE spectra in addition to the broadening σ_{total} to establish a quantitative representation of this subgap absorption (Table 1). In contrast to E_g fluctuations, Urbach tails may originate from phonon interactions and optical transitions between defect and tail states.¹⁸

As visible in Figure S3, the inclusion of Urbach tails leads to a flattening of the EQE onset and a corresponding broadening of the $dEQE/dE$ distribution. In contrast to the experimental EQE spectrum, fitting a Gaussian to a simulated $dEQE/dE$ distribution has the only purpose to determine the standard deviation (and not the effective E_g). As visible from Figure S3, the Gaussian fit to $dEQE/dE$ is not good; nevertheless, it allows for extracting a broadening via the standard

deviation. If this broadening were always included in the simulated EQE spectra, the determination of the individual impact of a CIGSe material property (E_g gradient, film thickness, and diffusion length) would be very complicated, and it would also cause conflict with the concept of disentanglement (Equation (1)). Therefore, we assume that the contribution of Urbach energy to the broadening is present in the component σ_{residual} and do not include any Urbach tails in simulated EQE spectra.

Apart from affecting the integral absorption of the incident sun light and thus the carrier collection of the solar cell, σ_{total} is detrimental to the device performance by leading to a decreased open-circuit voltage (V_{oc}).^{4,5}

$$\Delta V_{\text{oc}} = (\sigma_{\text{total}}^2)/(2ek_{\text{B}}T). \quad (2)$$

Here, k_{B} is Boltzmann constant, e is the elemental charge, and T is the absolute temperature of the solar cell. Note that Equation (2) provides the V_{oc} deficit due to radiative losses only. The gradient and the possible origins of σ_{residual} also lead to nonradiative recombination via defect states resulting in additional V_{oc} losses.

3 | MATERIALS AND METHODS

Solar cells fabricated at both ZSW, Stuttgart, Germany, and PVcomB, Berlin, Germany, were investigated. All photovoltaic parameters of the nine investigated cells are summarized in Table S4. At PVcomB, CIGSe layers were fabricated on Mo-coated soda lime glass (SLG) substrates following a three-stage-type thermal co-evaporation process as described in Heinemann et al.¹⁹ The range of substrate temperatures (T_s) was 500–650°C. The device had no antireflection coating. Other PVcomB absorbers were prepared by a sequential process using sputtered metal precursor layers, which were annealed in a nitrogen atmospheric pressure conveyor oven manufactured by Smit Thermal Solutions first, in Se vapor, and then in H_2S at 580–600°C.²⁰

At ZSW, CIGSe absorbers were deposited using an in-line multi-stage co-evaporation process on Mo-coated SLG substrates with an

TABLE 1 List of all solar cells investigated in more detail

Cell no.	E_g (eV)	σ_{total} (meV)	E_u (meV)	GGI	CGI	V_{oc} loss (mV)
1	1.02 ± 0.01	28 ± 2	17 ± 2	0.39 ± 0.03	0.88 ± 0.01	15 ± 2
2	1.03 ± 0.01	17 ± 2	12 ± 2	0.15 ± 0.02	0.94 ± 0.01	6 ± 3
3	1.03 ± 0.01	44 ± 2	14 ± 2	0.44 ± 0.01	0.93 ± 0.02	37 ± 3
4	1.1 ± 0.01	38 ± 2	18 ± 2	0.35 ± 0.02	0.93 ± 0.02	28 ± 2
5	1.1 ± 0.01	54 ± 2	19 ± 2	0.31 ± 0.01	0.85 ± 0.02	56 ± 3
6	1.18 ± 0.01	38 ± 2	19 ± 2	0.37 ± 0.02	0.94 ± 0.02	28 ± 2
7	1.19 ± 0.01	41 ± 2	20 ± 2	0.3 ± 0.02	0.87 ± 0.02	32 ± 2
8	1.19 ± 0.01	49 ± 2	26 ± 2	0.48 ± 0.02	0.84 ± 0.02	46 ± 3
9	1.2 ± 0.01	36 ± 2	16 ± 2	0.39 ± 0.02	0.91 ± 0.02	25 ± 2

Note: The GGI and CGI ratios for all the cells were calculated from the elemental concentrations measured by XRF. Solar cells having the same effective band-gap energy E_g in the CIGSe absorbers exhibited different standard deviations of $dEQE/dE$, σ_{total} . The V_{oc} loss was calculated using Equation 2, and E_u as described in Section 2.

industrially relevant 30 x 30 cm² coater.²¹ No additional alkali PDT process was used, and Na (partially K) was only provided from SLG during CIGS deposition at elevated temperatures. Integral GGI ratios of 0.30 and 0.66 as confirmed by X-ray fluorescence were realized by adapting the Ga and In evaporation rates on different substrate carriers in the same deposition run. Subsequently, the CdS buffer layer was grown on the CIGS absorbers by chemical bath deposition with a thiourea-based process. Radio-frequency-sputtered i-ZnO was deposited as highly resistive (HR) layer, and direct-current-sputtered ZnO:Al was used as front contact. Solar cells with a total area of 0.5 cm² were completed with Ni/Al/Ni grid fingers on top without antireflective coating.

EQE measurements were performed under light bias at zero and -1 V bias voltage over a wavelength range of 300 to 1400 nm, with silicon and indium gallium arsenide solar cells as references. The elemental distributions perpendicular to the substrate in the CIGSe layers were analyzed by means of glow-discharge optical emission spectroscopy (GDOES)²² and energy dispersive X-ray spectroscopy (EDX). EDX mapping was performed under an acceleration voltage between 7 and 10 kV, and the data were evaluated using Oxford Instruments Aztec software packages. (We do not show the EDX data in the present work since they provide the same elemental distributions as the GDOES results.) The average grain size distribution was determined by electron backscatter diffraction (EBSD). Also, the lateral emission fluctuation on micrometer scale was investigated via cathodoluminescence (CL) spectroscopy.²³ For EQE simulations ($\lambda = 300\text{--}1400$ nm) via SCAPS²⁴ (see Table S5 for simulation details), the absorption coefficient (α) in the absorption model was calculated considering the case of a direct gap semiconductor where

$$\alpha = A(h\nu - E_g)^{1/2} \quad (\text{for } h\nu \geq E_g) \quad (3)$$

Here, A is a material-dependent parameter calculated for every cell using their corresponding, integral $[\text{Cu}]/([\text{Ga}] + [\text{In}])$ (CGI) and GGI values.²⁵ For the device simulations via SCAPS, we varied the electron diffusion length (via the electron mobilities, the effective defect density, and the electron lifetimes in the CIGSe layer) or the absorber layer thickness or the GGI gradient perpendicular to the substrate (via the E_g gradient and that of the electron affinity, calculated from the gradient in GGI) as input parameters.

4 | RESULTS

4.1 | E_g and σ_{total} from experimental EQE for graded CIGSe absorbers

As a first step, the approach described in Section 2 (Figure 1) was applied to the EQE spectra acquired from 50 different CIGSe solar cells. We note that all the studied CIGSe absorber layers in these cells exhibited Ga/In gradients perpendicular to the substrate. In Figure 2, the extracted σ_{total} was plotted versus effective E_g (here, E_g is obtained from the mean of the Gaussian used to fit the E_g distribution and this corresponds with the local minimum of the E_g gradient).

In order to study systematically the influence of various CIGSe materials properties on σ_{total} , a series of nine CIGSe solar cells was analyzed in more detail. The effective E_g , the integral GGI and CGI ratios of the CIGSe absorber layer, as well as the extracted σ_{total} (Section 2) and the corresponding V_{oc} losses (Equation (2)) are given in Table 1. We note that the two cells with the largest σ_{total} , cell nos. 5 and 8, exhibit the lowest CGI ratios (0.85 and 0.84); as we will see further below (Table 2), these are also the two cells with the largest σ_{residual} values. Earlier work by Stephan et al.^{26,27} suggests that the density of point defects is higher the smaller the CGI ratio.

Nevertheless, a clear dependency of σ_{total} as a function of E_g cannot be detected; as already outlined in Section 2, various materials properties contribute to σ_{total} , of which E_g may be one. Notably, one solar cell with the smallest σ_{total} of 17 meV and $E_g = 1.03$ eV particularly stood out; this cell was further investigated in detail in the present work to reveal what the material properties of the CIGSe absorber layer are for such a low σ_{total} .

4.2 | Effect of the grading in CIGSe thin films

To investigate the effect of the E_g gradient (or Ga/In gradient) in CIGSe on the EQE onset (and thus, on the broadening of E_g distribution perpendicular to the substrate), again, SCAPS simulations were performed. We incorporated the experimental E_g gradients that are given in Figures 3 and S6. Every solar cell had a unique absorber thickness (Table 2), which was used in the SCAPS simulations.

To obtain a parameter representing the pattern of grading at the location of minimum E_g corresponding to the onset in the EQE spectrum, the curvature at the notch point was determined for all E_g

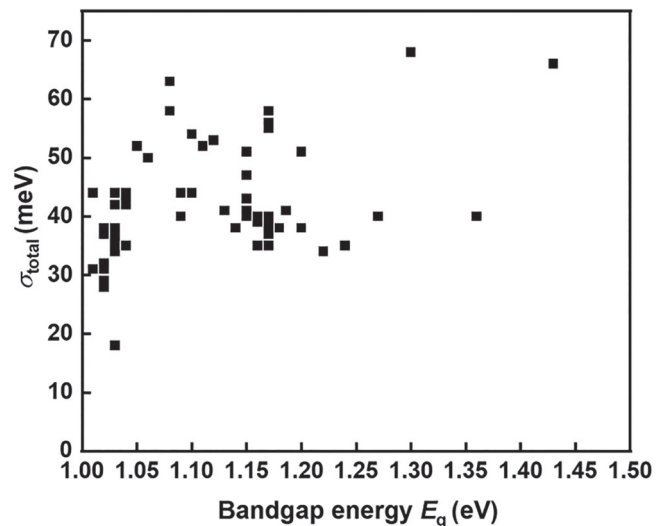
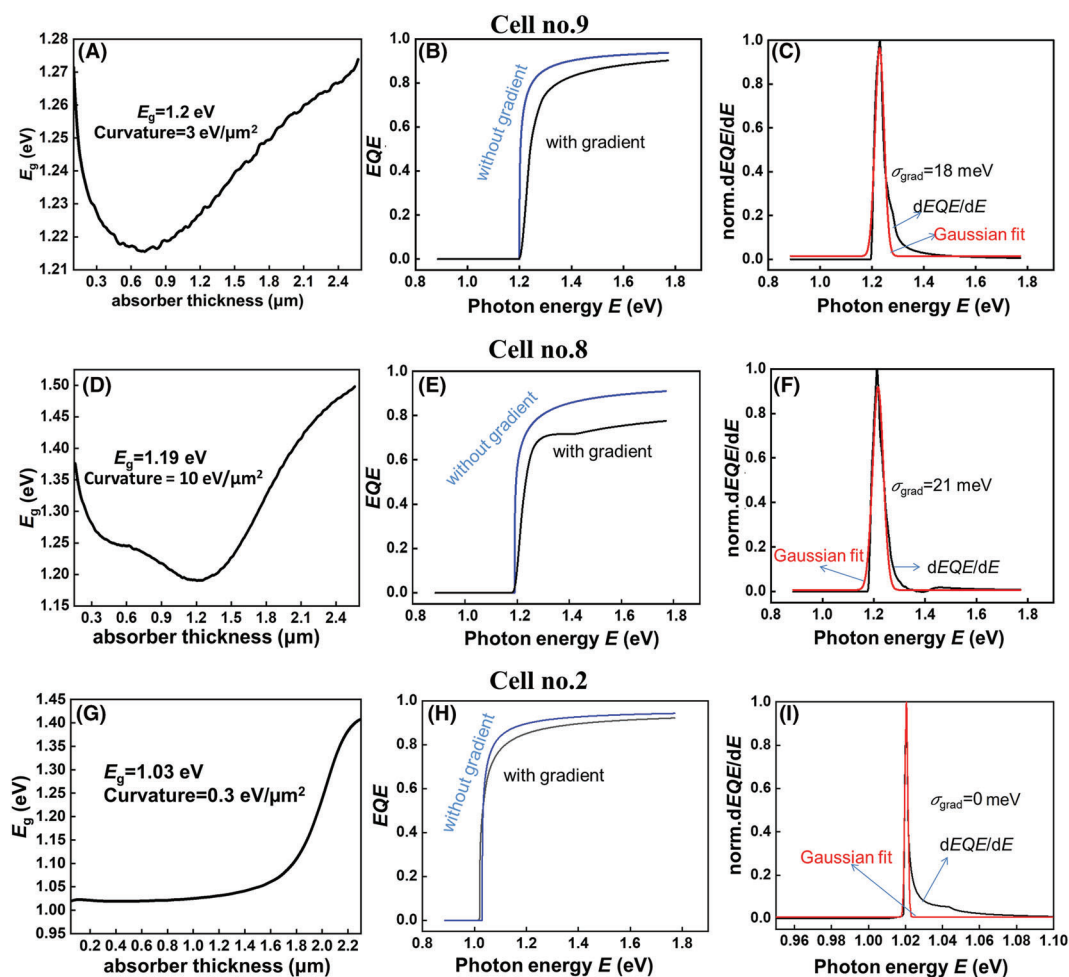


FIGURE 2 σ_{total} vs E_g from the approach depicted in Figure 1, showing no specific dependency of σ_{total} on E_g . One solar cell (cell no. 2 in Table 1) exhibits the smallest σ_{total} of 17 meV with effective E_g of 1.03 eV. The experimental errors in the extracted σ_{total} and E_g values are about 2 and 10 meV (about the size of the symbols)

TABLE 2 Calculated curvatures, σ_{grad} and residual component σ_{residual} for all investigated solar cells with different E_g and total CIGSe thickness

Cell no	E_g (eV)	Total CIGSe thickness (μm)	σ_{total} (meV)	Curvature ($\text{eV}/\mu\text{m}^2$)	σ_{grad} (meV)	σ_{residual} (meV)
1	1.02 ± 0.01	1.6 ± 0.1	28 ± 2	1.8 ± 0.1	21 ± 1	19 ± 2
2	1.03 ± 0.01	2.3 ± 0.1	17 ± 2	0.3 ± 0.1	0	17 ± 2
3	1.03 ± 0.01	1.7 ± 0.1	44 ± 2	2.3 ± 0.3	16 ± 1	41 ± 2
4	1.10 ± 0.01	2.3 ± 0.1	38 ± 2	5 ± 2	16 ± 1	34 ± 2
5	1.10 ± 0.01	2.6 ± 0.1	54 ± 2	9 ± 2	20 ± 1	50 ± 2
6	1.18 ± 0.01	2.7 ± 0.1	38 ± 2	5 ± 1	16 ± 1	34 ± 2
7	1.18 ± 0.01	2.0 ± 0.1	41 ± 2	2.0 ± 0.1	23 ± 1	34 ± 2
8	1.19 ± 0.01	2.3 ± 0.1	49 ± 2	10 ± 1	21 ± 1	44 ± 2
9	1.20 ± 0.01	2.5 ± 0.1	36 ± 2	3 ± 1	18 ± 1	31 ± 2

**FIGURE 3** (A, D, G) E_g gradients calculated from glow-discharge optical emission spectroscopy (GDOES) depth profiles for solar cell nos. 9, 8, and 2. Also given are the corresponding values for E_g and the curvature. (B, E, H) Simulated external quantum efficiency (EQE) and (C, F, I) Gaussian fitted $dEQE/dE$ for the cell nos. 9, 8, and 2 by using each of their original GGI gradient to model the CIGSe absorber. There is no broadening of the E_g distribution for homogeneous CIGSe layers; however, when a gradient is incorporated, there is a broadening of the $dEQE/dE$ for all the cells except for cell no.2 (with a rather flat gradient)

gradients. For a curve $f(x) = E_g(x)$ with x a position on an axis perpendicular to the substrate, the curvature at the local minimum of the E_g gradient is quantified by the second derivative $d^2f(x)/dx^2$.²⁸

The gradient as such has a considerable effect on the shape of the EQE and thus contributes correspondingly to σ_{total} . Cell nos.8 and 9 have identical E_g ; however, the shapes of their E_g gradients

are different. As shown in Figure 3D, cell no. 8 exhibits a stronger gradient and thus a larger broadening (Figure 3F) ($\sigma_{\text{grad}} = 21$ meV) when compared with cell no. 9 featuring a gradient with relatively smaller curvature (Figure 3A). For all the nine solar cells, σ_{grad} values were determined (see Table 2) by fitting Gaussians to the dEQE/dE dependencies (see Figure S6 for the remaining six cells). Cell no. 2 featuring a flat gradient with the lowest curvature has the smallest σ_{grad} of the order of 0.001 meV ($\sigma_{\text{grad}} \sim 0$ meV) (Figure 3I). The effect of the gradient on the EQE onset was further confirmed by modeling CIGSe layers of the same thickness and E_g but having gradients of various curvatures ranging from 0 to 4 eV/ μm^2 (see supporting information S7).

Cell no. 2 with the smallest σ_{total} of 17 meV exhibits a flat E_g gradient with curvature 0.3 eV/ μm^2 , that is, the minimum E_g was almost constant throughout a major part of the CIGSe absorber (Figure 3G). Overall, curvature values ranging from 0.3 (cell no. 2) to 10 eV/ μm^2 were obtained (see also Figure S6).

4.3 | Assessing the residual component σ_{residual}

Using the information of Section 4.2, we can now use Equation (1) and determine σ_{residual} . Table 2 lists the residual components σ_{residual} for these cells, together with the values for σ_{total} , the curvature, and σ_{grad} . The σ_{grad} values remain between 0 (cell no. 2) and 23 meV. The residual component σ_{residual} exhibits much larger values (25–50 meV) for all cells with the exception of cell no. 2 (17 meV).

It is important to note that a E_g gradient affects the broadening of the EQE onset in various ways. First, it contributes to σ_{grad} . In addition, a E_g gradient is always linked to microstructural and compositional variations perpendicular to the substrate that have a share in σ_{residual} .

In Table 2, there are solar cells that exhibit identical minimum E_g and different σ_{residual} values and again other cells with the same σ_{residual} but different E_g . In order to shed more light on how the CIGSe materials properties may affect σ_{residual} , we present case studies in the following Section 4.4, investigating selected solar cells (cell nos. 2, 8, and 9) more in detail by means of EBSD and CL (note that corresponding results from cell nos. 4 and 6 are provided in Figures S8 and S9).

4.4 | Case studies correlating the microstructure, the curvature, and the lateral fluctuations in luminescence emissions to the σ_{residual} of selected cells

4.4.1 | Cell no.2: $\sigma_{\text{residual}} = 17$ meV, $E_g = 1.03$ eV

This particular solar cell exhibits the smallest σ_{residual} of 17 meV and a flat E_g gradient (apart from the one at the back) in the CIGSe absorber (curvature 0.3 eV/ μm^2 ; see Figure 3G). As visible in Figure 4B, the CIGSe absorber exhibits large grains in the top region of the absorber, where the E_g (i.e., Ga/In) gradient remains flat and small grains only close to the Mo back contact, where the GGI ratio becomes much larger (the average grain size, d_{grain} , is about 0.5 μm including all grains in the absorber). We note that the dependency of the average grain size on the GGI ratio in the CIGSe layer was investigated in an earlier work.²⁹ The amplitude of the lateral fluctuations in the emission spectra of this cell was investigated via hyperspectral CL imaging with a pixel size of 50 nm. (Figure 4C). The fluctuations of the CL emission were analyzed parallel to the substrate at the positions of the notch in the E_g gradients by obtaining a standard deviation of the emission energy across 192 pixels. The minimum amplitude of fluctuations in the CL emission perpendicular to the substrate ($\sigma_{\text{CL,perp}}$) was also extracted by taking a standard deviation of the emission energy across

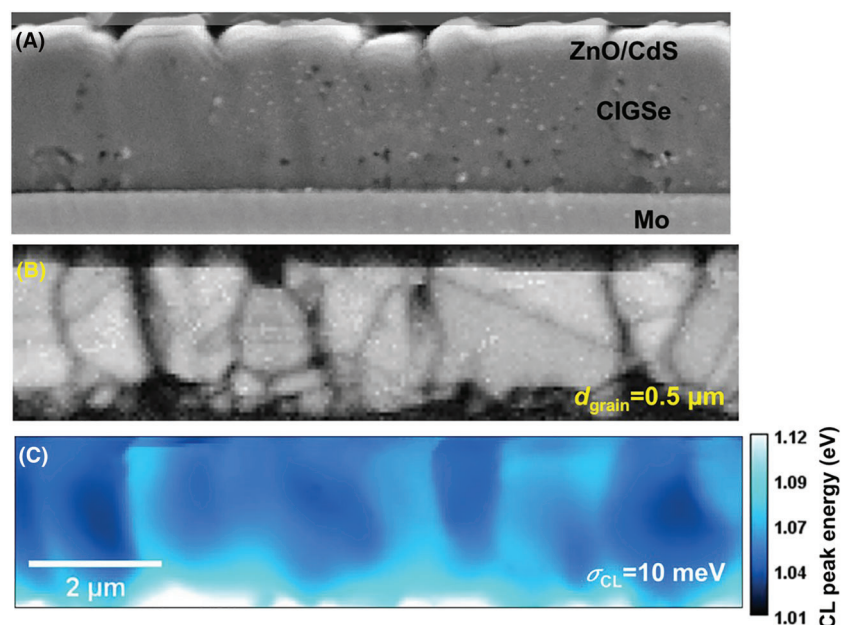


FIGURE 4 (A) Cross-section SEM image of the solar cell stack of cell no. 2. (B) Electron backscatter diffraction (EBSD) pattern-quality map from the same position. Larger grains are found in the top part of the CIGSe layer because of the flat Ga/In gradient, smaller grains towards the Mo back contact due to higher GGI. (C) Cathodoluminescence (CL) peak energy distribution map of the same position as in (A) and (B)

51 pixels (see also Table S10). From the CL peak energy distribution map (Figure 4C), it is apparent that the peak in the CL emission varies with the depth (owing to the Ga/In gradients) and also laterally. The CL emission occurs at higher energies towards the back contact because of the higher GGI ratio.

The lateral and perpendicular fluctuations of the CL emission exhibited very similar amplitudes $\sigma_{\text{CL,lateral}}$ and $\sigma_{\text{CL,perp}}$ of about 10 and 9 meV (see Table 3). This means that with hardly any compositional gradient present in the absorber, fluctuations with small amplitudes remain which seem to be isotropic in the CIGSe thin film and lead to only small, radiative V_{oc} losses.

4.4.2 | CIGSe solar cells with similar effective E_g but different σ_{residual} (cell no.8 with $\sigma_{\text{residual}} = 44$ meV, $E_g = 1.19$ eV and cell no.9 with $\sigma_{\text{residual}} = 31$ meV, $E_g = 1.20$ eV)

Cell nos.8 and 9 contain CIGSe layers with nearly the same (effective) E_g . However, the σ_{residual} value of cell no. 8 (44 meV) is higher by 14 meV than that of cell no. 9 (31 meV). This difference in σ_{residual} cannot be explained well via the slight differences in the lateral fluctuation of CL emission (σ_{CL} is 15 meV vs. 12 meV; see Figure 5C,F). In contrast, the average grain size of the CIGSe layer in cell no. 8 is 0.2 μm , while in cell no. 9, it is 0.4 μm . This difference is probably also linked to the difference in curvature values (10 and 3 $\text{eV}/\mu\text{m}^2$) and

elemental composition. We can assume considerable microstrain induced by the Ga/In gradients being present perpendicular to the substrate, as well as slight compositional variations and additional microstrain in the lateral directions, which is different for the CIGSe layers in cell nos.8 and 9.

5 | DISCUSSIONS

The evaluation of the EQE spectrum of a solar cell provides valuable insight into the limitations of the device performance. Apart from the direct link between the EQE spectrum and the short-circuit current density j_{sc} , the broadening of the EQE onset can be related to a radiative V_{oc} loss assessed by quantifying the standard deviation σ_{total} of the $d\text{EQE}/dE$ dependency. As apparent from the results further above, influences of the absorber thickness and the electron diffusion length on σ_{total} can be neglected. In contrast, the E_g gradient (perpendicular to the substrate) in the CIGSe layer as well as a residual component, attributed (at least in part) to E_g fluctuations, exhibit the two quantities contributing to σ_{total} .

It is convenient to divide the total broadening σ_{total} into its components σ_{grad} and σ_{residual} (Equation 1). The contribution of σ_{thick} and σ_{diff} can be neglected for nongraded absorbers with thicknesses above 1 μm and diffusion lengths larger than 1.5 μm . We found that σ_{grad} is substantial in case of large curvature values (>1 $\text{eV}/\mu\text{m}^2$), but that σ_{residual} is always larger than σ_{grad} .

TABLE 3 Summary correlating the grain size, the lateral fluctuations in CL emission, and the curvature with the σ_{residual} and radiative V_{oc} loss of selected cells

Cell no.	Curvature ($\text{eV}/\mu\text{m}^2$)	d_{grain} (μm)	$\sigma_{\text{CL,lateral}}$ (meV)	$\sigma_{\text{CL,perp}}$ (meV)	σ_{residual} (meV)	V_{oc} loss (mV)
2	0.3 ± 0.1	0.5 ± 0.05	10 ± 2	9 ± 2	17 ± 2	6 ± 3
6	5 ± 1	0.6 ± 0.05	12 ± 2	11 ± 2	34 ± 2	28 ± 2
9	3 ± 1	0.4 ± 0.05	12 ± 2	12 ± 2	31 ± 2	25 ± 2
4	5 ± 2	0.3 ± 0.05	13 ± 2	38 ± 3	34 ± 2	28 ± 2
8	10 ± 2	0.2 ± 0.05	15 ± 2	23 ± 2	44 ± 2	46 ± 3

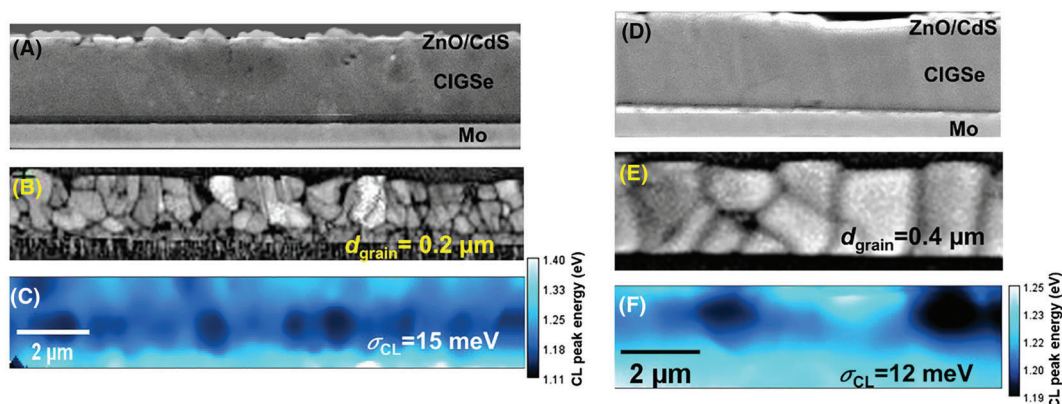


FIGURE 5 (A, D) SEM images of the investigated cross sections of cell nos. 8 (A) and 9 (D). (B, E) Electron backscatter diffraction (EBSD) pattern-quality maps from the same areas as in (A) and (D). (C, F) Cathodoluminescence (CL) peak energy distribution maps from the same areas as in (A) and (D). Pixel size = 50 nm

As for the CL emission, the amplitudes of fluctuations perpendicular to the substrate ($\sigma_{\text{CL,perp}}$) are always larger than those in lateral directions ($\sigma_{\text{CL,lateral}}$); see Tables 3 and S10. We can attribute this fact at least in part to the much larger compositional changes perpendicular to the substrate mainly due to the Ga/In gradient.

It is interesting to compare the curvature, the average grain size, and the amplitudes of fluctuations in CL emission of a CIGSe layer with the σ_{residual} value of the corresponding solar cell (Table 3). As visible from this comparison, σ_{residual} is increased with increasing curvature and with decreasing average grain size. Since the average grain size/the microstructure in general depends substantially on the Ga/In gradient and thus on the curvature, we can attribute a major contribution to σ_{residual} to local variations in composition and to (micro)strain perpendicular to the substrate, hence, by features which can be regarded as origins of E_{g} fluctuations.

In contrast, the $\sigma_{\text{CL,lateral}}$ values are very similar to each other; it is unclear whether the given differences (10–15 meV) are really significant. Within the scope of the present work, it was not possible to detect any significant variations in chemical composition in the lateral directions via EDX mapping; we were not able to distinguish unambiguously between possible compositional variations and statistical fluctuations in the elemental distribution maps.

A E_{g} -graded CIGSe absorber exhibits a gradual EQE onset resulting in a radiative V_{oc} loss, determined by the total broadening σ_{total} (containing contributions from σ_{grad} and σ_{residual}). In addition, the device performance can also be affected by the V_{oc} losses due to nonradiative recombination influenced strongly by the E_{g} gradients in the CIGSe layer perpendicular to the substrate, since they affect the microstructure and hence the density of grain boundaries in the polycrystalline absorber, which act as centers of enhanced (nonradiative) recombination.³⁰ Overall, the V_{oc} deficit due to radiative recombination is quantified by σ_{total} (containing σ_{grad} and σ_{residual}) and not only by σ_{residual} .

At this point, we would like to note that Ga/In gradients in the CIGSe layer in the regions close to the front and back contacts are known to be beneficial with respect to reducing interface recombination at these interfaces.³¹ However, we emphasize that a flat E_{g} gradient (with small curvature) spanning across a major depth of the CIGSe layer³² leads not only to enhanced absorption and collection but also to reduced broadening σ_{total} , thus smaller radiative V_{oc} losses.

6 | CONCLUSION

In the present work, we investigated the effect of various material properties of CIGSe absorbers on the onsets of EQE spectra of corresponding solar cells. Compositional gradients perpendicular to the substrate in the CIGSe thin films were identified as substantial contributors to the broadening of these EQE onsets, leading to radiative V_{oc} losses. Flat E_{g} gradients across a major depth of the CIGSe layer yield steep EQE onsets and thus smaller current and voltage losses in the corresponding solar cells. The present work gives hints of

how to change the materials design of CIGSe absorbers for power conversion efficiencies of 25% and beyond.

ACKNOWLEDGEMENTS

The authors are grateful to Ulrike Bloeck (HZB) for assistance with the SEM specimen preparation. The present work was supported by the Graduate School “MatSEC” and the BMWK-funded project “EFFCIS-II” under contract numbers O3EE1059A (ZSW) and O3EE1059B (HZB). Special thanks are due to Thomas Unold and Susan Schorr, HZB, for fruitful discussions. Open access funding enabled and organized by Projekt DEAL.

ORCID

Tobias Bertram  <https://orcid.org/0000-0002-4060-7523>

Christian Kaufmann  <https://orcid.org/0000-0001-9168-2032>

Tim Kodalle  <https://orcid.org/0000-0002-8792-9669>

José A. Márquez Prieto  <https://orcid.org/0000-0002-8173-2566>

Hannes Hempel  <https://orcid.org/0000-0001-9689-9644>

Leo Choubrac  <https://orcid.org/0000-0003-3236-6376>

Wolfram Witte  <https://orcid.org/0000-0002-9429-506X>

Dimitrios Hariskos  <https://orcid.org/0000-0003-4867-1578>

Roland Mainz  <https://orcid.org/0000-0003-4793-9763>

Romain Carron  <https://orcid.org/0000-0001-8281-4881>

Jan Keller  <https://orcid.org/0000-0002-3461-6036>

Pablo Reyes-Figueroa  <https://orcid.org/0000-0001-9262-1645>

Reiner Klenk  <https://orcid.org/0000-0003-2045-4301>

Daniel Abou-Ras  <https://orcid.org/0000-0003-3063-922X>

REFERENCES

- Nakamura M, Yamaguchi K, Kimoto Y, Yasaki Y, Kato T, Sugimoto H. Cd-free Cu(In,Ga)(Se,S)₂ thin-film solar cell with record efficiency of 23.35%. *IEEE J Photovolt*. 2019;9(6):1863-1867. doi:10.1109/JPHOTOV.2019.2937218
- Alonso MI, Wakita K, Pascual J, Garriga M, Yamamoto N. Optical functions and electronic structure of CuInSe₂, CuGaSe₂, CuInS₂, and CuGaS₂. *Phys. Rev. B - Condens Matter Mater Phys*. 2001;63(7):075203. doi:10.1103/PhysRevB.63.075203
- Heise SJ, Gerliz V, Hammer MS, Ohland J, Keller J, Hammer-Riedel I. Light-induced changes in the minority carrier diffusion length of Cu (In,Ga)Se₂ absorber material. *Sol Energy Mater sol Cells*. 2017;163:270-276. doi:10.1016/j.solmat.2017.01.045
- Mattheis J, Rau U, Werner JH. Light absorption and emission in semiconductors with band gap fluctuations-A study on Cu (In,Ga)Se₂ thin films. *J Appl Phys*. 2007;101(11):1-11, 113519. doi:10.1063/1.2721768
- Werner JH, Mattheis J, Rau U. Efficiency limitations of polycrystalline thin film solar cells: Case of Cu (In,Ga)Se₂. *Thin Solid Films*. 2005;480-481:399-409. doi:10.1016/j.tsf.2004.11.052
- Wei SH, Zhang SB, Zunger A. Effects of Ga addition to CuInSe₂ on its electronic, structural, and defect properties. *Appl Phys Lett*. 1998;72(24):3199-3201. doi:10.1063/1.121548
- Rau U, Blank B, Müller TCM, Kirchartz T. Efficiency potential of photovoltaic materials and devices unveiled by detailed-balance analysis. *Phys Rev Appl*. 2017;7(4):044016. doi:10.1103/PhysRevApplied.7.044016
- Rau U, Werner JH. Radiative efficiency limits of solar cells with lateral band-gap fluctuations. *Appl Phys Lett*. 2004;84(19):3735-3737. doi:10.1063/1.1737071

9. Chantana J, Kawano Y, Nishimura T, Mavlonov A, Minemoto T. Impact of Urbach energy on open-circuit voltage deficit of thin-film solar cells. *Sol Energy Mater sol Cells*. 2020;210:110502. doi:[10.1016/j.solmat.2020.110502](https://doi.org/10.1016/j.solmat.2020.110502)
10. Carron R, Andres C, Avancini E, et al. Bandgap of thin film solar cell absorbers: A comparison of various determination methods. *Thin Solid Films*. 2019;669:482-486. doi:[10.1016/j.tsf.2018.11.017](https://doi.org/10.1016/j.tsf.2018.11.017)
11. Nikolaeva A, Krause M, Schäfer N, et al. Electrostatic potential fluctuations and light-soaking effects in Cu (In,Ga)Se₂ solar cells. *Prog Photovoltaics Res Appl*. 2020;28(9):919-934. doi:[10.1002/pip.3299](https://doi.org/10.1002/pip.3299)
12. Richter M, Hammer MS, Sonnet T, Parisi J. Bandgap extraction from quantum efficiency spectra of Cu (In,Ga)Se₂ solar cells with varied grading profile and diffusion length. *Thin Solid Films*. 2017;633:213-217. doi:[10.1016/j.tsf.2016.08.022](https://doi.org/10.1016/j.tsf.2016.08.022)
13. Ren Y, Scragg JJS, Frisk C, Larsen JK, Li SY, Platzer-Björkman C. Influence of the Cu₂ZnSnS₄ absorber thickness on thin film solar cells. *Phys Status Solidi Appl Mater Sci*. 2015;212(12):2889-2896. doi:[10.1002/pssa.201532311](https://doi.org/10.1002/pssa.201532311)
14. Rai M, Wong LH, Etgar L. Effect of Perovskite Thickness on Electroluminescence and Solar Cell Conversion Efficiency. *J Phys Chem Lett*. 2020;11(19):8189-8194. doi:[10.1021/acs.jpcclett.0c02363](https://doi.org/10.1021/acs.jpcclett.0c02363)
15. Mattheis J. Mobility and homogeneity effects on the power conversion efficiency of solar cells, Diss. University of Stuttgart (2006) [10.18419/opus-2638](https://doi.org/10.18419/opus-2638)
16. Dietrich J, Abou-Ras D, Schmidt SS, et al. Origins of electrostatic potential wells at dislocations in polycrystalline Cu (In,Ga)Se₂ thin films. *J Appl Phys*. 2014;115(10):103507. doi:[10.1063/1.4867398](https://doi.org/10.1063/1.4867398)
17. Abou-Ras D, Schäfer N, Hages CJ, Levchenko S, Márquez J, Unold T. Inhomogeneities in Cu (In,Ga)Se₂ thin films for solar cells: Band-gap versus potential fluctuations. *Sol RRL*. 2018;2(1):1700199. doi:[10.1002/solr.201700199](https://doi.org/10.1002/solr.201700199)
18. Wasim SM, Rincón C, Marín G, et al. Effect of structural disorder on the Urbach energy in Cu ternaries. *Phys. Rev. B - Condens Matter Mater. Phys*. 2001;64(19):195101.
19. Heinemann MD, Mainz R, Österle F, et al. Evolution of optoelectronic properties during film formation of complex semiconductors. *Sci Rep*. 2017;7(1):1-9, 45463. doi:[10.1038/srep45463](https://doi.org/10.1038/srep45463)
20. Schmidt SS, Wolf C, Rodríguez-Alvarez H, et al. Adjusting the Ga grading during fast atmospheric processing of Cu (In,Ga)Se₂ solar cell absorber layers using elemental selenium vapor. *Prog Photovoltaics Res Appl*. 2017;25(5):341-357. doi:[10.1002/pip.2865](https://doi.org/10.1002/pip.2865)
21. Powalla M, Voorwinden G, Hariskos D, Jackson P, Kniese R. Highly efficient CIS solar cells and modules made by the co-evaporation process. *Thin Solid Films*. 2009;517(7):2111-2114. doi:[10.1016/j.tsf.2008.10.126](https://doi.org/10.1016/j.tsf.2008.10.126)
22. Kodalle T, Greiner D, Brackmann V, et al. Glow discharge optical emission spectrometry for quantitative depth profiling of CIGS thin-films. *J Anal at Spectrom*. 2019;34(6):1233-1241. doi:[10.1039/C9JA00075E](https://doi.org/10.1039/C9JA00075E)
23. Abou-Ras D, Kirchartz T, Rau U. *Advanced Characterization Techniques for Thin Film Solar Cells*. Weinheim, Germany: Wiley; 2016. doi:[10.1002/9783527699025](https://doi.org/10.1002/9783527699025).
24. Burgelman M, Nollet P, Degraeve S. Modelling polycrystalline semiconductor solar cells. *Thin Solid Films*. 2000;361:527-532. doi:[10.1016/S0040-6090\(99\)00825-1](https://doi.org/10.1016/S0040-6090(99)00825-1)
25. Carron R, Avancini E, Feurer T, et al. Refractive indices of layers and optical simulations of Cu (In,Ga)Se₂ solar cells. *Sci Technol Adv Mater*. 2018;19(1):396-410. doi:[10.1080/14686996.2018.1458579](https://doi.org/10.1080/14686996.2018.1458579)
26. Stephan C, Schorr S, Tovar M, Schock HW. Comprehensive insights into point defect and defect cluster formation in CuInSe₂. *Appl Phys Lett*. 2011;98(9):1-3, 091906. doi:[10.1063/1.3559621](https://doi.org/10.1063/1.3559621)
27. Stephan C, Scherb T, Kaufmann CA, Schorr S, Schock HW. Cationic point defects in CuGaSe₂ from a structural perspective. *Appl Phys Lett*. 2012;101(10):1-4, 101907. doi:[10.1063/1.4751338](https://doi.org/10.1063/1.4751338)
28. Tu LW. *Differential Geometry*. Vol. 275. Springer; 2017. doi:[10.1007/978-3-319-55084-8](https://doi.org/10.1007/978-3-319-55084-8).
29. Abou-Ras D, Caballero R, Kaufmann CA, et al. Impact of the Ga concentration on the microstructure of CuIn_{1-x}Ga_xSe₂. *Phys Stat. Sol. (RRL)*. 2008;2(3):135-137. doi:[10.1002/pssr.200802059](https://doi.org/10.1002/pssr.200802059)
30. Krause M, Nikolaeva A, Maiberg M, et al. Microscopic origins of performance losses in highly efficient Cu (In,Ga)Se₂ thin-film solar cells. *Nat Commun*. 2020;11(1):4189. doi:[10.1038/s41467-020-17507-8](https://doi.org/10.1038/s41467-020-17507-8)
31. Feurer T, Reinhard P, Avancini E, et al. Progress in thin film CIGS photovoltaics. *Prog Photovolt: Res Appl*. 2017;25(7):645-667. doi:[10.1002/pip.2811](https://doi.org/10.1002/pip.2811)
32. Edoff M, Jarmar T, Nilsson NS, et al. High V_{oc} in (Cu,Ag)(In,Ga)Se₂ solar cells. *44th IEEE PVSC*. 2017;7(6):1789-1794.

SUPPORTING INFORMATION

Additional supporting information may be found in the online version of the article at the publisher's website.

How to cite this article: Thomas S, Bertram T, Kaufmann C, et al. Effects of material properties of band-gap-graded Cu(In,Ga)Se₂ thin films on the onset of the quantum efficiency spectra of corresponding solar cells. *Prog Photovolt Res Appl*. 2022;1-9. doi:[10.1002/pip.3572](https://doi.org/10.1002/pip.3572)